# Effect of random variations in microstructure on the development of final creep failure in polycrystalline aggregates

Giessen, E. van der; Tvergaard, V.

*Published in:*
Modelling and Simulation in Materials Science and Engineering

*DOI:*
10.1088/0965-0393/2/3A/020

Modelling Simul. Mater. Sci. Eng. 2 (1994) 721–738. Printed in the UK

# Effect of random variations in microstructure on the development of final creep failure in polycrystalline aggregates

E van der Giessen† and V Tvergaard‡

† Laboratory for Engineering Mechanics, Delft University of Technology, Delft, The Netherlands

‡ Department of Solid Mechanics, The Technical University of Denmark, Lyngby, Denmark

Received 4 November 1993, accepted for publication 4 November 1993

**Abstract.** Planar analyses of a unit cell containing many grains are used to study the effect of random variations in the microstructure on failure times in a metal subject to creep at high temperatures. The model accounts for intergranular failure by cavity nucleation and growth to coalescence, or by grain boundary sliding, and the deformations of the grains are represented by power-law creep and elasticity. Two kinds of microstructural variations are considered: variations in the size and shape of grains, and variations in the cavity nucleation properties. Failure times are determined for various levels of deviation from a uniform periodic array of hexagonal grains. For variations in grain geometry, the times are correlated with the relative change in the average density of grain boundary facets, while the variance of the distribution is used for the simulations with random nucleation properties. For each case analysed, the time to first cavity coalescence as well as the time to final failure by link-up of grain boundary microcracks are determined.

## 1. Introduction

Creep fracture in polycrystalline metals at elevated temperatures occurs mainly by intergranular cavitation and microcracking. Cavities nucleate and grow most rapidly on grain boundary facets normal to the maximum principal stress direction (e.g. [1, 2]), and facet microcracks form by coalescence of cavities. Several micromechanical studies of creep failure have focused on the time to cavity coalescence on a characteristic grain boundary facet (e.g. see [3–6]), thus neglecting the remaining part of the lifetime required for the linking-up of these microcracks to form the final macroscopic crack. Most of these studies have considered axisymmetric model problems, which give a reasonably realistic approximation of the real three-dimensional facet geometry, but are not well suited for link-up studies.

Plane-strain models of a polycrystalline aggregate give a less accurate description of real facet geometries than can be obtained by axisymmetric or full 3D models. However, such planar models have the attractive feature that they can be used to obtain insight in the linking-up process, as has been done by van der Giessen and Tvergaard [7, 8], first for a unit cell covering two neighbouring grains, and recently for a larger unit cell containing many hexagonal grains. The larger unit cell, accounting for grain boundary sliding as well as the nucleation and growth of cavities on grain boundary facets, has also been used by van der Giessen and Tvergaard [9] to study the effect of distribution and density of facets subject to early cavitation. Hsia *et al* [10] have used such a cell model with free sliding

0965-0393/94/3A0721+18$19.50  

but no cavitation to study the effect of microcrack density on the rate of opening of a facet microcrack. In the recent study [8], for a cell containing many hexagonal grains, failure times have been determined for a material with essentially *no voids initially, in which* a material inhomogeneity is represented by one central grain boundary facet having more rapid cavity nucleation than the other grain boundaries. In this multi-grain cell model the first microcrack forms at the grain boundary facet with more rapid cavity nucleation, and subsequently microcracks form at other facets. Finally, these microcracks link up by the combined influence of cavitation and grain boundary sliding on intermediate inclined grain boundary facets. Thus, it was possible to determine the part of the total lifetime spent in the final linking-up process.

In the present paper, the planar multi-grain unit cell model is used to investigate the effect of random variations in the size and shape of the grains, and random variations in the rate of cavity nucleation on the different grain boundary facets. When models focus on materials consisting of a periodic array of uniform hexagonal grains, it is usually assumed that the chosen grain size and shape represents an average for the material, and that also the corresponding lifetimes are representative of the behaviour of the real material. The analyses to be discussed here give an estimate of the validity of such assumptions.

## 2. Material model for creep cavitation

The material model used in this study accounts for (i) elastic and creep deformation of the grains, (ii) viscous grain boundary sliding and (iii) the nucleation and growth of grain boundary cavities to coalescence. The resulting non-linear problem, based on constitutive equations to be presented shortly, will be analysed by means of a finite-strain, convected coordinate formulation of the governing field equations. In such a formulation, $g_{ij}$ and $G_{ij}$ denote the metric tensors in the reference and current deformed configurations, respectively, with determinants $g$ and $G$, and the Lagrangian strain tensor has components $\eta_{ij}$. The contravariant components $\tau^{ij}$ of the Kirchhoff stress tensor on the current base vectors are defined in terms of the Cauchy stress tensor components $\sigma^{ij}$ by $\tau^{ij} = \sqrt{G/g}\,\sigma^{ij}$.

The total strain rate within each grain is taken to be the sum of the elastic part $\dot{\eta}^{\mathrm{E}}_{ij}$ and the creep part $\dot{\eta}^{\mathrm{C}}_{ij}$. Thus, with the usual elastic stress–strain relationship $\overset{\nabla}{\tau}{}^{ij} = R^{ijkl}\dot{\eta}^{\mathrm{E}}_{kl}$, in terms of the Jaumann stress rate $\overset{\nabla}{\tau}{}^{ij} = \dot{\tau}^{ij} + (G^{ik}\tau^{jl} + G^{jk}\tau^{il})\dot{\eta}_{kl}$, the constitutive relations for the elastic-creeping grain material can be written as

$$\overset{\nabla}{\tau}{}^{ij} = R^{ijkl}(\dot{\eta}_{kl} - \dot{\eta}^{\mathrm{C}}_{kl}).$$

The creep part of the Lagrangian strain rate accounts for power-law creep, and is given by

$$\dot{\eta}^{\mathrm{C}}_{ij} = \dot{\epsilon}^{\mathrm{C}}_{\mathrm{e}}\frac{3}{2}\frac{s_{ij}}{\sigma_{\mathrm{e}}} \qquad \dot{\epsilon}^{\mathrm{C}}_{\mathrm{e}} = \dot{\epsilon}_0\left(\frac{\sigma_{\mathrm{e}}}{\sigma_0}\right)^n \tag{2.1}$$

where $\dot{\epsilon}_0$ and $\sigma_0$ are reference strain-rate and stress quantities, and $n$ is the creep exponent. The effective Mises stress $\sigma_{\mathrm{e}} = (\frac{3}{2}\tau_{ij}\tau^{ij})^{1/2}$ and the stress deviator $s^{ij} = \tau^{ij} - \frac{1}{3}G^{ij}\tau^k_k$ are specified directly in terms of the Kirchhoff stresses $\tau^{ij}$, thus neglecting the relative volume change $\sqrt{G/g} - 1$ due to elastic strains which remain small.

According to Ashby [11] grain boundaries can be modelled as thin layers that slide in a linear viscous manner such that the relative sliding velocity $\dot{u}$ of adjacent grains due to a shear stress $\tau$ in the grain boundary is given as

$$\tau = \eta_{\mathrm{B}}\dot{u}/w \tag{2.2}$$

where $w$ is the thickness of the boundary. He also gives an explicit relation for the viscosity $\eta_B$ of an idealized boundary, while Raj and Ashby [12] give corrections on the value of the viscosity due to various kinds of irregularities in the grain boundary. For the present purpose, $\eta_B/w$ is regarded as a separate material parameter, which can be specified conveniently in terms of the strain-rate-like parameter [6, 13]

$$\dot{\epsilon}_B = \dot{\epsilon}_0 \left[ \left( 2\sqrt{3} \frac{R_0}{w} \eta_B \frac{\dot{\epsilon}_0}{\sigma_0} \right)^{n/(n-1)} \right]^{-1}.$$

Here, $R_0$ is a reference length parameter which we shall later on identify as the average grain facet radius (or, the half facet size in a planar polycrystal model). Thus, free grain boundary sliding is characterized by $\dot{\epsilon}_c^C/\dot{\epsilon}_B = 0$, while $\dot{\epsilon}_c^C/\dot{\epsilon}_B \to \infty$ in the limit of no sliding.

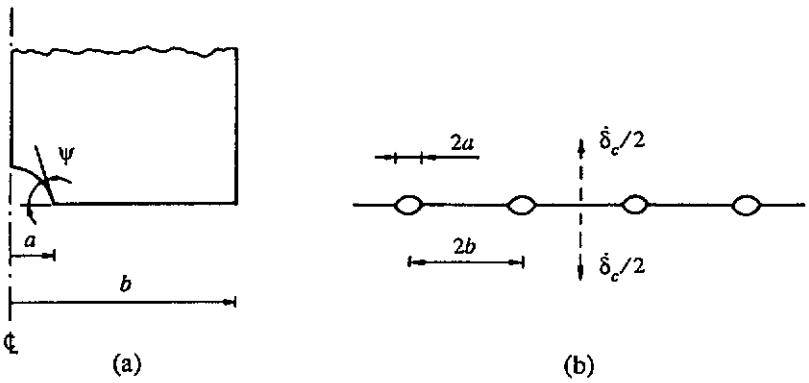


**Figure 1.** (*a*) Geometry of a cavity in the spherical-caps shape; (*b*) equally spaced cavities on a grain boundary.

Cavities on grain boundaries are assumed to maintain the quasi-equilibrium spherical-caps shape (see figure 1). This assumption is widely accepted for so-called transverse grain boundary facets, i.e. facets that are normal to the maximum principal tensile stress direction. However, on grain boundaries that are inclined to the maximum principal tensile stress direction, and therefore prone to grain boundary sliding, diffusional growth accompanied by grain boundary sliding may give rise to non-equilibrium void shapes. As in previous investigations, we will neglect the effect on the growth rate of individual cavities; according to [6], this is a reasonable approximation for relatively low sliding rates. Spherical-caps-shaped cavities can be specified by their radius $a$, average spacing $2b$ and cavity tip angle $\psi$. The latter will be taken as $\psi = 75°$ in the following. The average separation between adjacent grains due to the presence of cavities of size $a$ and half-spacing $b$ is $\delta_c = V/(\pi b^2)$, where $V$ is the cavity volume given by $V = \frac{4}{3}\pi a^3 h(\psi)$ in terms of the cavity shape parameter $h(\psi) = [(1+\cos\psi)^{-1} - \frac{1}{2}\cos\psi]/\sin\psi$. Based on experimental data (e.g. [14, 15]), it is assumed that the cavity spacing is much smaller than the facet length. With this approximation, the grain boundary cavities can be represented in terms of a continuous variation of $a$ and $b$, and therefore of $V$ and $\delta_c$. Recognizing, moreover, that cavitation need not be uniform over a grain boundary facet, these cavitation parameters are allowed to vary over each grain boundary facet.

The grain boundary cavities grow by diffusion as well as by creep of the surrounding grain material. For a transverse grain boundary facet, approximate expressions for the growth rate have been developed on the basis of detailed numerical studies of the coupled growth problem reported in detail in [4, 16, 17]. Thus, the volumetric growth rate $\dot{V}$ of a single cavity of radius $a$ and half-spacing $b$ is expressed as

$$\dot{V} = \dot{V}_1 + \dot{V}_2 \quad \text{for } a/L \leqslant 10 \qquad f = \max\left[\left(\frac{a}{b}\right)^2, \left(\frac{a}{a+1.5L}\right)^2\right] \tag{2.3}$$

where

$$\dot{V}_1 = 4\pi\mathcal{D}\frac{\sigma_n - (1-f)\sigma_s}{\ln(1/f) - \frac{1}{2}(3-f)(1-f)} \tag{2.4}$$

$$\dot{V}_2 = \begin{cases} \pm 2\pi\dot{\epsilon}_e^C a^3 h(\psi)[\alpha_n|\sigma_m/\sigma_e| + \beta_n]^n & \pm\sigma_m/\sigma_e > 1 \\ 2\pi\dot{\epsilon}_e^C a^3 h(\psi)[\alpha_n + \beta_n]^n \sigma_m/\sigma_e & |\sigma_m/\sigma_e| \leqslant 1. \end{cases} \tag{2.5}$$

Here, $\mathcal{D} = D_B\delta_B\Omega/kT$ is the grain boundary diffusion parameter, with $D_B\delta_B$ denoting the boundary diffusivity, $\Omega$ the atomic volume, $k$ Boltzmann's constant and $T$ the absolute temperature. Furthermore, $\sigma_n$ is the average stress normal to the current orientation of the grain boundary in the vicinity of the void, while $\sigma_m$ and $\sigma_e$ are the average mean and Mises stress, respectively. The sintering stress $\sigma_s$ in (2.4) will be neglected. The constants appearing in (2.5) are given by $\alpha_n = 3/2n$ and $\beta_n = (n-1)(n+0.4319)/n^2$. The parameter

$$L = (\mathcal{D}\sigma_e/\dot{\epsilon}_e^C)^{1/3}$$

in (2.3) has been introduced by Needleman and Rice [16] and serves as a stress- and temperature-dependent length scale governing the coupling between diffusive and creep contributions to void growth. For large values of this length scale, say $a/L < 0.1$, cavity growth is dominated by diffusion, while for larger values of $a/L$ creep growth becomes more and more important. As a consequence, cavity growth in situations where $a/L < 0.1$ or so is likely to be constrained by creep of the surrounding material, whereas this creep constraint reduces with increasing $a/L$ (see [3, 4, 17, 18]). With $\dot{V}$ according to (2.3) the growth rate of the cavity radius is obtained through $\dot{a} = \dot{V}/(4\pi a^2 h(\psi))$.

The cavity spacing, represented by $b$, changes in the course of the failure process due to the nucleation of new cavities and, to a lesser extent, due to finite-strain effects associated with the in-plane deformations. Introducing the number of cavities per unit undeformed grain boundary area $N$, it follows that

$$\dot{b}/b = \tfrac{1}{2}(\dot{\epsilon}_1 + \dot{\epsilon}_2) - \tfrac{1}{2}\dot{N}/N \tag{2.6}$$

where $\dot{\epsilon}_1$ and $\dot{\epsilon}_2$ are the in-plane principal logarithmic strain rates at the grain boundary. The nucleation of new cavities, represented by $\dot{N}/N$, is a complex and not yet well-understood process, and therefore we employ a rather simplistic model, which is motivated by experimental observations (e.g. [2, 19]) which show that the number of cavities grows continuously with effective strain. Following earlier work [5, 9] we assume nucleation to be governed by the nucleation law

$$\dot{N} = F_n(\sigma_n/\Sigma_0)^2\dot{\epsilon}_e^C \tag{2.7}$$

with material constants $F_0$ and $\Sigma_0$. In (2.7), however, $\dot{\epsilon}_e^C$ is taken to be the local effective strain rate at the grain boundary which will in general be different for different boundary facets. Furthermore, this expression includes a dependence on the local facet stress $\sigma_n$ of the type suggested in [19], which allows the nucleation to be fastest on the highly stressed facets even if the local creep rates are the same. As discussed in detail in [5], we also assume that freshly nucleated, small cavities at a certain point grow so fast relative to already present cavities that the time needed to reach their size can be neglected. The expressions (2.3)–(2.7) determine the rate of change of the average separation $\delta_c$ between adjacent grains as

$$\dot{\delta}_c = \frac{\dot{V}}{\pi b^2} - \frac{2V}{\pi b^2}\frac{\dot{b}}{b}. \tag{2.8}$$

When the ratio $a/b$ approaches unity, coalescence of cavities occurs by failure of the ligament between cavities. It was noted in [1] that actual coalescence may already take place around $a/b \approx 0.5$ when the ligaments fail by ductile tearing or cleavage. Indeed, experimental data in [20] for various materials under various stress and temperature conditions suggest that the average value of $a/b$ on the fracture surface is roughly in the range of 0.4–0.6. The results to be reported here have been obtained by using $a/b = 0.7$ as the critical value for coalescence. Since cavitation over a grain boundary facet will usually develop in a non-uniform manner, coalescence will first take place at some location and this microcrack will subsequently propagate over the rest of the facet, until a full-facet microcrack has developed.

## 3. Problem formulation and numerical method

The development of creep failure is studied in terms of a 2D model of a polycrystalline material that has been proposed and used by the authors in previous studies [8, 9]. We recapitulate the basic features of the model for consistency, but refer to these references for further details. The planar model material is built up as an array of hexagonal grains, as shown in figure 2. In previous studies it was assumed that the grains were shaped as perfectly regular hexagons, as depicted in figure 2, but here we will allow for irregular hexagonal grains, as will be discussed later. It is assumed that the microstructure—in terms of grain shape, distribution of cavitating grain boundary facets, nucleation properties, etc—reflects a certain periodicity that allows for the identification of a unit cell with which the entire polycrystal can be built up by elementary translations. Let $2A_0$, $2B_0$ be the dimensions of the unit cell in the $x^1$ and $x^2$ directions, respectively, and let the cell contain $m_1 \times m_2$ grains (the cell shown in figure 2 is characterized by $(m_1, m_2) = (6, 5)$). In the case of regular hexagonal grains with facet width $2R_0$, the dimensions can be written as $A_0 = \frac{3}{2}R_0 m_1$, $B_0 = \sqrt{3}R_0 m_2$. Furthermore it is assumed that the cell itself exhibits reflection symmetry in the $x^1$ and $x^2$ directions, so that only one quadrant needs to be analysed. Due to symmetries, the four faces of the quarter unit cell will remain straight and aligned with the coordinate axes, and will not support any shear stress.

The polycrystal is taken to be subjected to a stationary macroscopic stress state specified by principal true stresses $\Sigma_1$ and $\Sigma_2$ under plane-strain conditions. The stress state is considered to be defined such that $x^2$ is the maximal principal tensile stress direction. With $\dot{u}^i$ and $T^i$ denoting the velocity components and the nominal traction components in the

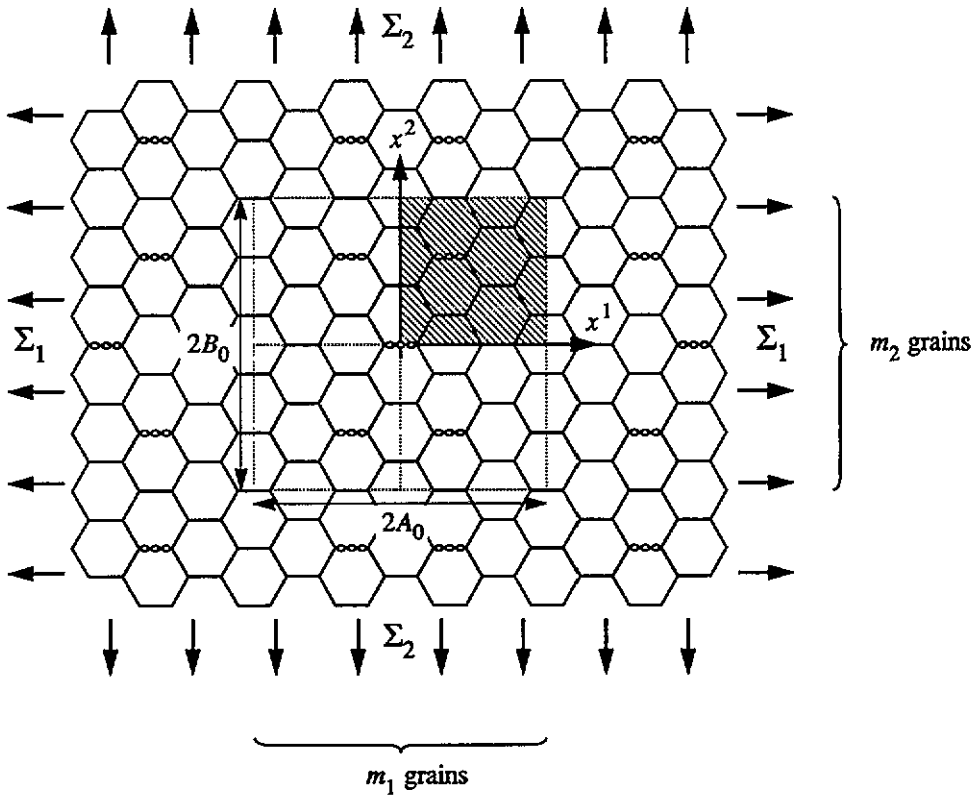


**Figure 2.** The two-dimensional periodic polycrystal model. The dashed rectangle indicates the $2A_0$ by $2B_0$ unit cell comprising $m_1 \times m_2$ grains. Only the hatched quadrant is analysed.

reference configuration, the boundary conditions applied to one quadrant of the unit cell then read

$$\begin{aligned} &\dot{u}^1 = 0 && T^2 = 0 && \text{along } x^1 = 0 \\ &\dot{u}^1 = \dot{U}_{\mathrm{I}} && T^2 = 0 && \text{along } x^1 = A_0 \\ &\dot{u}^2 = 0 && T^1 = 0 && \text{along } x^2 = 0 \\ &\dot{u}^2 = \dot{U}_{\mathrm{II}} && T^1 = 0 && \text{along } x^2 = B_0. \end{aligned}$$

The uniform velocities $\dot{U}_{\mathrm{I}}$ and $\dot{U}_{\mathrm{II}}$ are determined so that the average stresses $\Sigma_1$ and $\Sigma_2$, computed from

$$\Sigma_1 = \frac{1}{B}\int_0^{B_0} T^1\big|_{x^1=A_0}\,\mathrm{d}x^2 \qquad \Sigma_2 = \frac{1}{A}\int_0^{A_0} T^2\big|_{x^2=B_0}\,\mathrm{d}x^1$$

respectively, retain prescribed constant values. Here, $A = A_0 + U_{\mathrm{I}}$ and $B = B_0 + U_{\mathrm{II}}$ are the current deformed dimensions of the cell.

Any grain boundary facet in the polycrystal model may in principle be subject to cavitation, but cavitation on some facets may be faster or may take place earlier in the lifetime than on others. In [9] we studied the interactions among a few cavitating facets

normal to the $\Sigma_2$ direction. In [8], we proceeded beyond that by studying the entire failure process from an essentially low density of cavitating facets up to complete failure. In those studies, the polycrystal was built up from purely hexagonal grains with basically identical cavitation properties along all facets. The failure process was initiated by assuming an initial 'imperfection' in the form of the central grain boundary facet in the unit cell, transverse to the maximum principal stress $\Sigma_2$, being already microcracked or exhibiting a ten times higher nucleation factor $F_n$ in the nucleation law (2.7), so that the damage process starts at the centre of the unit cell. In the present study we wish to further extend the study of the failure process by considering a more or less random microstructure instead of an almost uniform one. Two aspects are considered to be randomly distributed in the polycrystal model, namely the shape and size of the grains, and, secondly, the nucleation activity at the grain facets expressed by the factor $F_n$ in the nucleation law (2.7).

The grains in the planar polycrystal model can in principle have any convex polygonal shape, provided that the symmetry conditions implied by the unit cell concept are respected. An obvious parameter to characterize the geometry of the microstructure would be the facet density $\rho$ defined by

$$\rho = \frac{1}{A_0 B_0} \sum_k R^{(k)2} \tag{2.9}$$

where the summation extends over all grain boundary facets in the quarter unit cell. Here, $A_0B_0$ is the area of a quarter of the unit cell (see figure 2) and $R^{(k)}$ is the half-facet width of facet $k$. Note that the parameter $\rho$, used here to characterize cavitating grain boundary facets, is similar to the crack density parameter introduced by Budiansky and O'Connell [21], and scales with the root mean square facet length. For a polycrystal built up of regular hexagonal grains with half-facet size $R_0$, the definition (2.9) reduces to $\rho = N_f R_0^2$ (where $N_f$ is the number of cavitating facets per unit area) which was used in previous studies [8, 9]. For reference it is noted that, in the case of regular hexagonal grains, the density is $\rho = 0.289$ if all facets are cavitating, while the density is only a third of that, $\rho = 0.096$, when only those facets transverse to the maximum principal stress direction, $\Sigma_2$, are cavitating. In this density parameter $\rho$ all facet orientations are accounted for with equal relative weight. On the other hand, it is well known that cavitation occurs preferentially on transverse facets due to the fact that the normal stress $\sigma_n$ is the primary driving force for cavity growth, as seen in (2.4). A measure of the density of cavitating facets that incorporates their orientation is a second-order density tensor whose components with respect to the (initial) $x^i$ coordinates are defined by

$$\alpha_{ij} = \frac{1}{A_0 B_0} \sum_k R^{(k)2} n_i^{(k)} n_j^{(k)}$$

where $n_i^{(k)}$ are the components of the unit normal vector to the $k$th facet in the initial configuration. This tensor is similar to Kachanov's [22] microcrack density tensor. The connection with the scalar-valued cavity density $\rho$ simply is $\rho = \alpha_{kk}$, while $\alpha_{22}$ is the component that relates to the density of transverse facets.

As discussed also in [8] and [9], care must be exercised in interpreting the results of this 2D model. Anderson and Rice [23] pointed out that the deformation of a grain in a real 3D polycrystalline aggregate is much more constrained by the surrounding grains than in the planar model considered here. An important inherent feature of the 2D polycrystalline aggregate is that, in the case of regular hexagonal grains with completely free grain boundary

sliding, it falls apart immediately when facet cracks have developed on all transverse grain boundaries (i.e. for $\rho = 0.096$), whereas the corresponding 3D aggregate has not yet completely lost its load-carrying capacity. It has been noted also [8] that complete failure of such a freely sliding 2D aggregate may already occur at a lower facet crack density, namely at the instant where a percolation of transverse facet cracks has developed running from the bottom to the top face of the cell such that conglomerates of grains slide off without resistance. If the grains in the 2D aggregate do not have the perfect hexagonal shape, deformations may be somewhat more constrained by surrounding grains. Also, in that case, it is not to be expected that the aggregate will fall apart immediately at densities around $\rho = 0.096$, since the various sliding directions are not aligned. However, the ensuing deformation rates are expected to be excessive and give a negligible contribution to the failure time.

The numerical procedure used to simulate the failure process in this planar polycrystal model has been outlined in some detail in [6] and [9], and will be only briefly recapitulated here. All grains in the polycrystal are modelled by a mesh consisting of quadrilateral finite elements, each being built up of four linear displacement triangular subelements arranged in a 'crossed triangle' configuration. Cavitation is treated by employing a 'smeared out' model, in which each grain facet with its discrete distribution of cavities of radius $a$ and half-spacing $b$ is replaced by a grain boundary layer with continuous distributions $a(x)$, $b(x)$ along the layer. The average separation between grains, $\delta_c(x)$, defines the thickness of this grain boundary layer. Special grain boundary elements are used to implement the cavitation process and the associated thickening of the boundary layer, according to (2.8), as well as to account for viscous grain boundary sliding, according to (2.2). For computational reasons, fictitious layers of linear elastic springs are added to the grain boundary layers: one with a normal stiffness $k_n$ and one with a tangential stiffness $k_s$. The normal stress $\sigma_n$ and shear stress $\tau$ at the grain boundary are then governed by the following constitutive equations:

$$\dot{\sigma}_n = k_n(\dot{\delta} - \dot{\delta}_c) \qquad \dot{\tau} = k_s(\dot{v} - \dot{v}_v)$$

with $\dot{\delta}$ and $\dot{v}$ being the actual normal thickening rate and relative sliding velocity, respectively, and with the inelastic components $\dot{\delta}_c$ and $\dot{v}_v$ being given by way of (2.8) and (2.2), respectively. Using large values of the stiffnesses of the fictitious elastic layers ensures that the deviations $\dot{\delta} - \dot{\delta}_c$ and $\dot{v} - \dot{v}_v$ are kept small: $k_n = k_s \approx 10E/R_0$ with $E$ being Young's modulus of the grain material.

The governing equations for the grains as well as the grain boundary layers are formulated within a linear incremental framework based on an incremental version of the virtual work equation. An equilibrium correction is applied to prevent drifting of the solution from the true equilibrium path. A forward gradient approach proposed in [24] was applied both to the creep constitutive equations (2.1) and to the constitutive equations describing cavitation and grain boundary sliding, to increase the stable step size (see [6] and [9]).

## 4. Results

As mentioned before, we consider two aspects of randomness in the microstructure: firstly, random variations in the geometry of the grains in the polycrystalline aggregate, and, secondly, a random distribution of nucleation activities at the grain boundary facets. In section 4.1 we will consider polycrystals with a random variation in grain geometries but

with uniform nucleation properties, while in section 4.2 we will study the effect of a random nucleation activity in a polycrystal with perfect hexagonal grains. The main purpose of these studies is to gain insight into how and how strongly such kinds of variations affect the times to failure. Of course, both types of randomness could be taken into account simultaneously, but we have chosen not to present such studies.

The parameters used in this study are in most cases identical to the parameters used in previous studies [6–9]. All cases to be presented are for a material with $\nu = 0.3$ and a creep exponent $n = 5$. The creep parameter $\dot{\epsilon}_0/\sigma_0^n$ is specified through the reference time $t_R = \Sigma_e/(E\dot{\epsilon}_e^C)$. Here, $E$ is Young's modulus, and $\Sigma_e$ and $\dot{\epsilon}_e^C$ are the macroscopic, applied effective Mises stress and the corresponding creep rate according to (2.1), respectively. The effective stress $\Sigma_e$ corresponding to the applied stresses $\Sigma_1$ and $\Sigma_2$ (see figure 2) is approximated by the expression $\Sigma_e = \frac{1}{2}\sqrt{3}|\Sigma_2 - \Sigma_1|$ for pure plane-strain creep. Most cases to be presented here have assumed uniaxial tension, $\Sigma_1 = 0$, but a few results have been obtained for a biaxial stress with $\Sigma_1 = 0.5\Sigma_2$. In all cases, the value of the applied stress $\Sigma_2$ is prescribed such that $\Sigma_e/E = 0.5 \times 10^{-3}$, so that the reference time is the same as in previous studies [7–9]. The grain boundary viscosity is specified through the value of $\dot{\epsilon}_B$ relative to the macroscopic creep rate $\dot{\epsilon}_e^C$. In this paper we confine attention to a single cell size, specified by $(m_1, m_2) = (6, 5)$ and by $A_0/B_0 = \frac{1}{2}\sqrt{3}m_1/m_2$. The corresponding half-facet width for a polycrystal with regular hexagonal grains is denoted by $R_0$ and will be used henceforth as a reference length parameter. The initial cavitation state for all facets is taken to be identical and uniform over the facet, and specified by the initial cavity size $a_I/R_0 = 0.01$ and by the initial spacing $b_I/R_0 = 1$. Recalling that $2R_0$ is the initial width of a facet in the regular planar model of figure 2, we note that if the facet were penny-shaped as in an axisymmetric model, this spacing would correspond to an initial density of $N_I = 1/(\pi R_0^2)$. The value $F_n = 100N_I$ is used as a reference value for the nucleation activity $F_n$ in (2.7), and the scaling parameter $\Sigma_0$ is chosen equal to $\Sigma_e$. The grain boundary diffusion parameter $\mathcal{D}$ in (2.4) is specified in terms of the length scale $L$ measured relative to the initial cavity radius $a_I$ by the initial value $(a/L)_I = 0.025$. For this value of $\mathcal{D}$, previous studies (e.g. [4, 5, 9]) have shown that cavity growth tends to be strongly constrained by the creep deformations of the surrounding grains during most of the lifetime.

### *4.1. Random variations in the geometry of grains*

In this section, we consider creep failure in (6, 5) unit cells of a single size but with various variations in the geometry of the constituent grains. The actual microstructures are generated in the following manner. The starting point is a (6, 5) unit cell with regular hexagonal cells, as studied extensively in previous work [8, 9]. Then the positions of the vertices of the grains are displaced at random within a circular region of a certain radius $\Delta R$ around the initial position. Special care is given to vertices of grains that intersect one of the four cell boundaries in order to maintain symmetry. A number of realizations have been considered for values of $\Delta R$ ranging from $0.3R_0$ to $0.9R_0$ (see figure 3). For each realization, the mean facet width was computed as well as the cavitating facet densities $\rho$ and $\alpha_{ij}$. The mean facet widths differed less than 2.5% from $R_0$. In the analyses, the material properties are taken to be the same for all grain boundary facets, as mentioned previously; the nucleation activity on all facets was taken to be specified by $F_n = 100N_I$.

The finite element mesh was generated by mapping each grain to a reference, regular hexagonal grain, then creating the mesh and finally mapping back to the actual grain. As an example, figure 4 shows the mesh for one of the irregular microstructures considered,

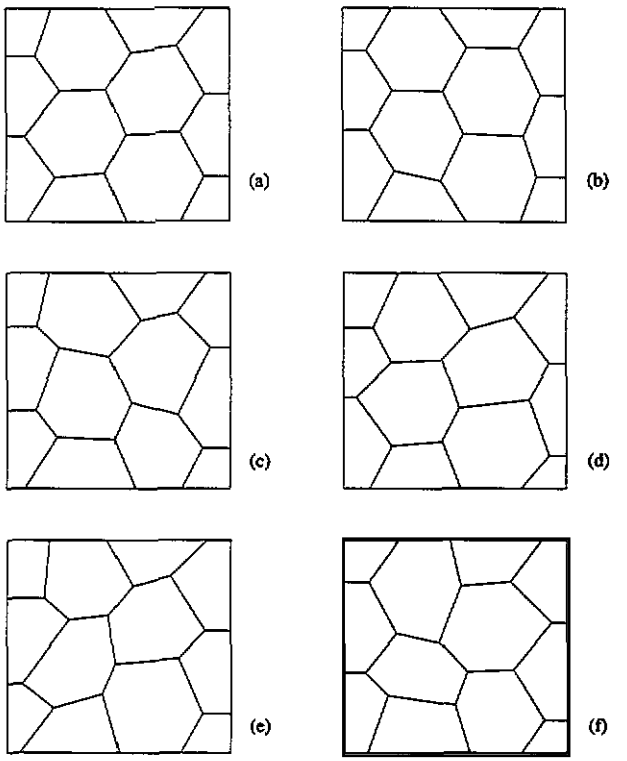


**Figure 3.** Different realizations of random variations in the geometry of grains inside a quarter of the unit cell. (*a*), (*b*) $\Delta R/R_0 = 0.3$, (*c*) $\Delta R/R_0 = 0.6$, (*d*) $\Delta R/R_0 = 0.75$, (*e*), (*f*) $\Delta R/R_0 = 0.9$.

namely the one shown in figure 3(*d*). Note that a refinement of the mesh is used along each grain boundary for describing microcrack propagation.

First let us consider the development of final failure for cases where there is free grain boundary sliding. As an illustration, figure 5 shows the failure development for the microstructure of figure 3(*d*). The figures show 'snapshots' of the cavitation state within the quarter cell at different stages of the failure process normalized by the ultimate time to failure $t_f$. This is done in the following way. The value of $a/b$ along each facet is plotted perpendicular to that facet and with the ordinate along the facet. In fact, $a/b$ is plotted on both sides of the facet in order to be able to represent the damage evolution when the adjacent grains slide relative to each other. In principle, the values of $a/b$ plotted on either side at a particular point should be identical, but due to the time and spatial discretization this cannot be achieved exactly. The regions where microcracking has occurred due to cavity coalescence at $a/b = 0.7$ are highlighted by a darker gray level.

The first stage, shown in figure 5(*a*), corresponding to about 75% of the final lifetime, displays that grain boundary cavitation has indeed developed in a rather non-uniform manner due to the irregular microstructure. As expected, grain boundary facets that are close to the transverse direction, i.e. normal to the $\Sigma_2$ direction, have accumulated most damage. Cavity coalescence has occurred first at the facet in the top right-hand corner of the cell, which also microcracked first just before this instant. Microcracking has already started from the triple points at another facet of relatively small width, which is located on the vertical

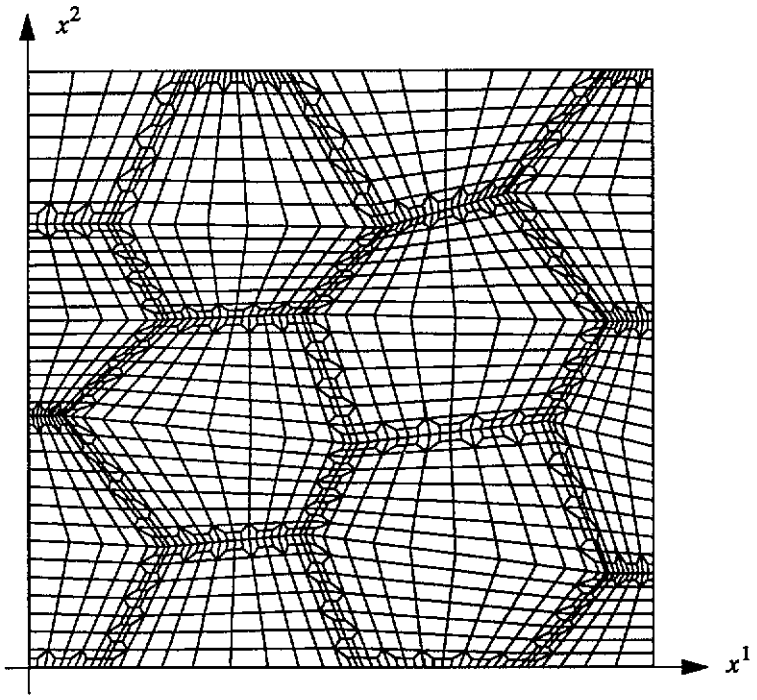


**Figure 4.** Finite element mesh used in the numerical analyses of a quadrant of the (6, 5) unit cell corresponding to figure 3(*d*). Each quadrilateral is composed of four triangular constant-strain subelements.

axis of symmetry of the unit cell. At the next stage, figure 5(*b*), that facet has also failed completely, and the microcracks start to link up by microcracking of facets in between. Cavitation damage now becomes very non-uniform with large regions that are effectively shielded by the present microcracks (figure 5(*c*)). At this stage, the failure process proceeds extremely rapidly, and the last stage shown in figure 5(*d*) is just before final failure. It is seen that during the last stages of the lifetime, some cavitation also develops on the grain boundaries that are well inclined to the applied stress direction, but final failure of the aggregate occurs predominantly by the grains sliding off. For the other microstructures analysed, the actual failure pattern is of course different, but the main characteristics are similar. Cavity coalescence and microcracking tends to occur first at small grain facets, which are then linked-up by microcracking of intermediate facets.

Figure 6 summarizes the results of computations with each of the microstructures of figure 3 in terms of three landmarks in the lifetime of the material: the time $t_c$ to first cavity coalescence, the time $t_{cr}$ to the first full facet microcrack, and the final time to complete loss of integrity $t_f$. The specific microstructures used are identified by (*a*)–(*f*) according to figure 3. In figure 6(*a*) the times are plotted against the deviation $\Delta\rho$ of the facet density $\rho$ with respect to the value $\rho_0 = 0.289$ for the microstructure with regular hexagonal grains. Similarly, in figure 6(*b*), they are plotted against the difference $\Delta\alpha_{22}$ in the 22-component of the density tensor $\alpha_{ij}$ with respect to the value $\alpha_{22}^0 = 0.144$ for regular hexagonal grains. It is seen that all random variations of grain geometry considered yield a reduction of the failure times. Also notice that the time between first coalescence and final failure is influenced significantly by variations in the microstructure. The microstructure

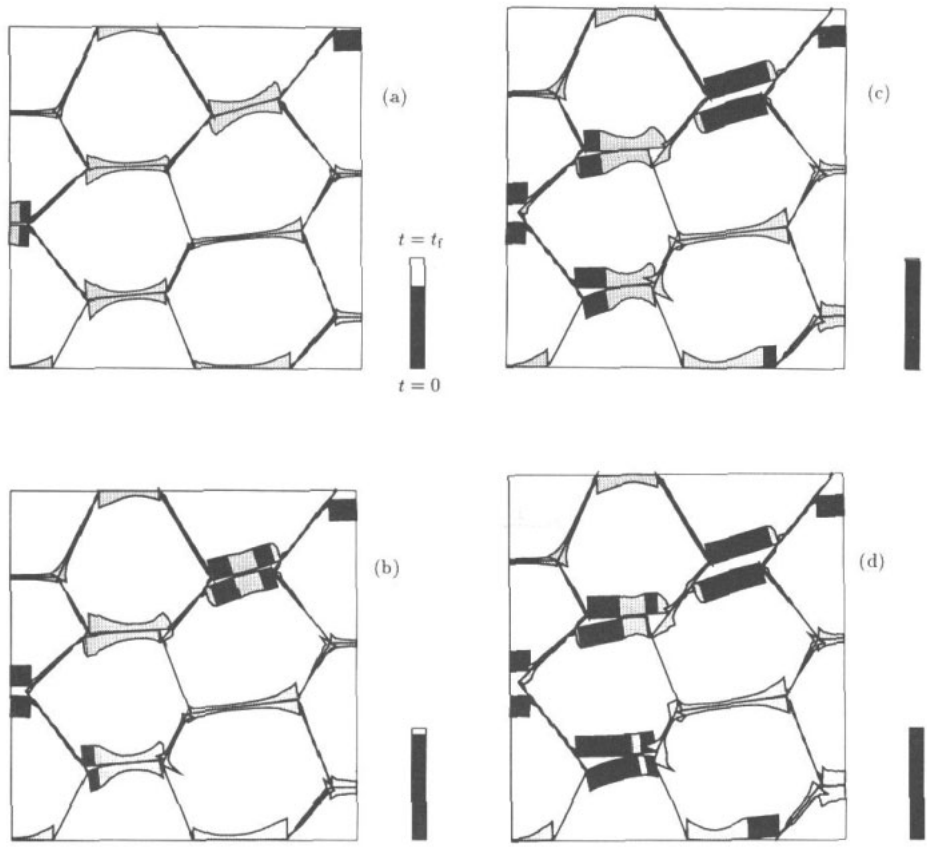


**Figure 5.** The state of damage at different stages $t/t_f$ in a quarter unit cell with the microstructure of figure 3(*d*) with free grain boundary sliding for $\Sigma_1 = 0$. Values of $a/b$ are plotted along, and on either side of, the grain boundary facets, and microcracked regions where $a/b = 0.7$ are indicated by the darker gray scale. (*a*) $t/t_f = 0.75$, (*b*) $t/t_f = 0.94$, (*c*) $t/t_f = 0.99$, (*d*) $t/t_f \approx 1$.

of figure 3(*e*) clearly gives the most drastic reduction: compared to the regular hexagonal microstructure, $t_f$ has been lowered by a factor of around 4. The linear regression lines of the $t_f$ data suggest a strong dependence of the failure time to geometric variations in the microstructure.

The analyses have been repeated for some microstructures by assuming a stress state where $\Sigma_1 = 0.5\Sigma_2$, but for the same parameters otherwise as before. In [8] we studied the influence of this higher triaxiality stress state on the failure development in polycrystals with regular hexagonal grains; it was found that, obviously, the times to failure are different but that the failure pattern was essentially similar to that for uniaxial tension. This is also found here for the polycrystals with random grain variations. Comparing the characteristic times, shown in figure 7, with the corresponding ones for uniaxial tension in figure 6, one first observes that the times have been roughly halved; this is readily explained from the fact that, for the same value of the applied Mises stress $\Sigma_e$, the applied principal stress $\Sigma_2$ is half of that in uniaxial tension. Furthermore, the variation of failure times with increasing randomness in grain geometry expressed in terms of $\Delta\rho$ is seen to be similar to that under uniaxial tension.

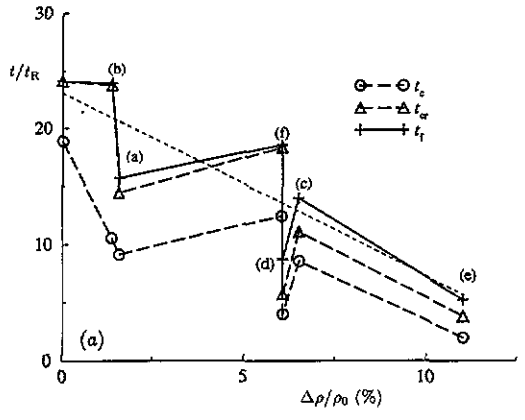


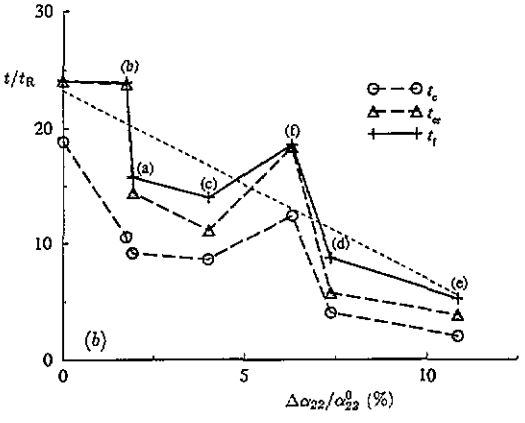


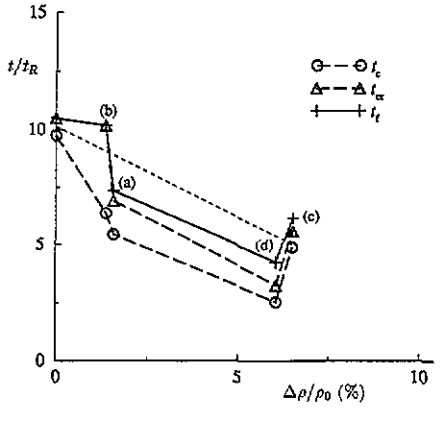


**Figure 6.** Times to first coalescence, $t_c/t_R$, times to first facet microcrack, $t_{cr}/t_R$, and times to failure, $t_f/t_R$, for the (6, 5) unit cells of figure 3 with free grain boundary sliding for $\Sigma_1 = 0$. Results are plotted against $\Delta\rho/\rho_0$ in (*a*) and against $\Delta\sigma_{22}/\sigma_{22}^0$ in (*b*). *The thin broken line is* a linear regression of the times to failure, $t_f$, and markers (a)–(f) indicate the different microstructures shown in figure 3.

**Figure 7.** Times to first coalescence, $t_c/t_R$, times to first facet microcrack, $t_{cr}/t_R$, and times to failure, $t_f/t_R$, for the (6, 5) unit cells of figure 3 with free grain boundary sliding for $\Sigma_1 = 0.5\Sigma_2$. Results are plotted against $\Delta\rho/\rho_0$ *and the thin broken line is a linear regression* of the times to failure $t_f$. Markers (a)–(f) indicate the different microstructures shown in figure 3.

In the foregoing analyses the grains were able to slide freely against each other. Previous work (e.g. [6, 8, 9]) has revealed that creep constraints on cavitation and the associated stress redistributions during cavitation and microcrack propagation are rather sensitive to the grain boundary viscosity. In order to gain some insight into the influence of that on the sensitivity of failure to random variations in the microstructure, we have repeated the above computations for uniaxial tension with a large value of the boundary viscosity corresponding to $\log(\dot{\epsilon}_e^C/\dot{\epsilon}_B) = 3.5$, such that sliding is practically prohibited [8, 9]. Figure 8 illustrates the failure development in the microstructure shown in figure 3(*d*) in the absence of sliding. The first stage shown in figure 8(*a*) at about 95% of the lifetime shows that cavitation on nearly transverse facets has developed rather uniformly. There is much less preference for certain facets than in the corresponding case with free grain boundary sliding (figure 5). At somewhat later stages, shown in figures 8(*b*) and (*c*), cavitation is seen to spread even more

uniformly over nearly transverse facets. Only when most of these facets have microcracked, does coalescence and microcracking occur on inclined facets, much like in the case of regular hexagonal grains.

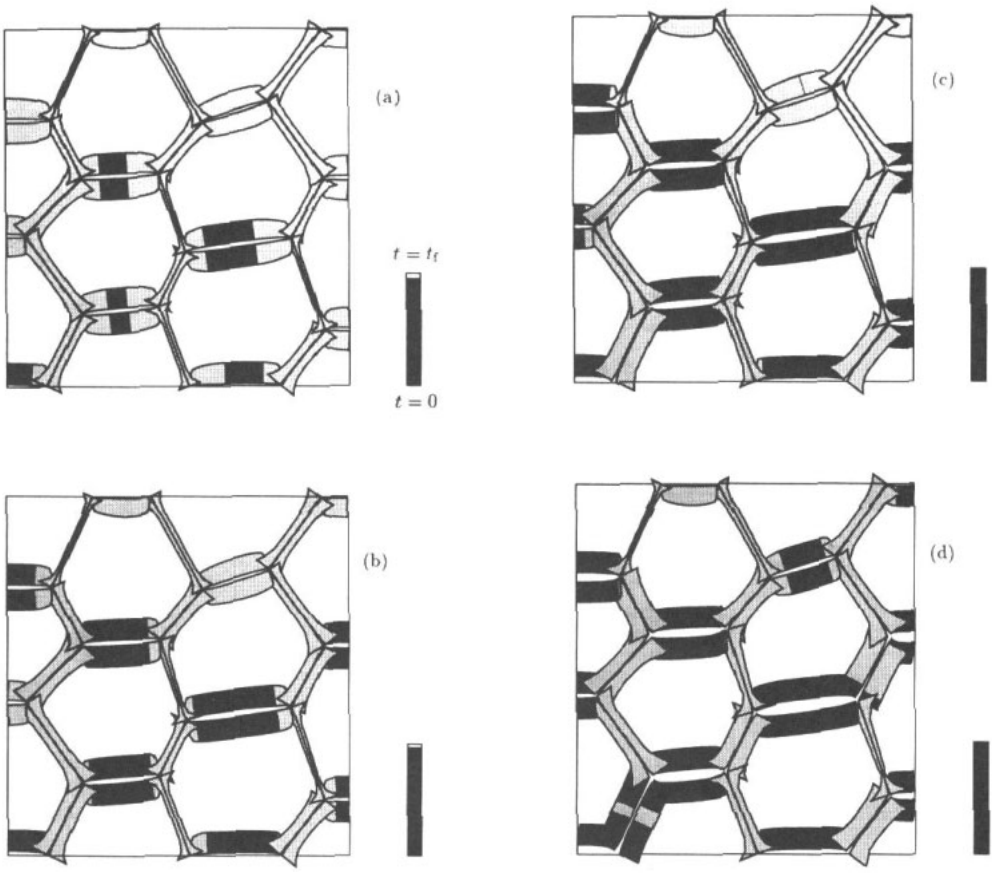


**Figure 8.** The state of damage at different stages $t/t_f$ in a quarter unit cell with the microstructure of figure 3(*d*) with no grain boundary sliding for $\Sigma_1 = 0$. (*a*) $t/t_f = 0.95$, (*b*) $t/t_f = 0.97$, (*c*) $t/t_f = 0.99$, (*d*) $t/t_f \approx 1$.

Figure 9 confirms that without grain boundary sliding, the characteristic failure times are not affected much by random variations in the microstructure. Linear regression seems to indicate that the time to failure $t_f$ reduces slightly with $\Delta\rho$, but the small number of cases analysed of course does not admit any statistically meaningful conclusions. The results also seem to suggest that the difference between the time to coalescence and the time to failure decreases with increasing randomness.

### *4.2. Random variation in nucleation activity*

This section focuses on creep failure in (6, 5) unit cells built up with regular hexagonal grains, as in [8], but with randomly attributed values of the nucleation activity parameter $F_n$ in the nucleation law (2.7). A value of $F_n$ is assigned to each facet by randomly selecting a

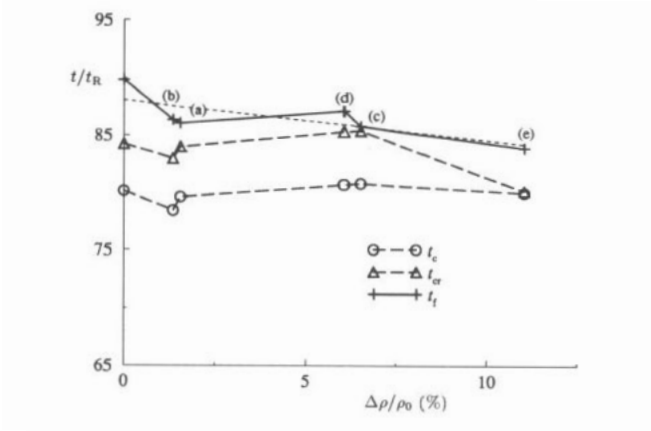


**Figure 9.** Times to first coalescence, $t_c/t_R$, times to first facet microcrack, $t_{cr}/t_R$, and times to failure, $t_f/t_R$, for the (6, 5) unit cells of figure 3 with no grain boundary sliding for $\Sigma_1 = 0$. Results are plotted against $\Delta\rho/\rho_0$, and the thin broken line is a linear regression of the times to failure $t_f$. Markers (a)–(f) indicate the different microstructures shown in figure 3.

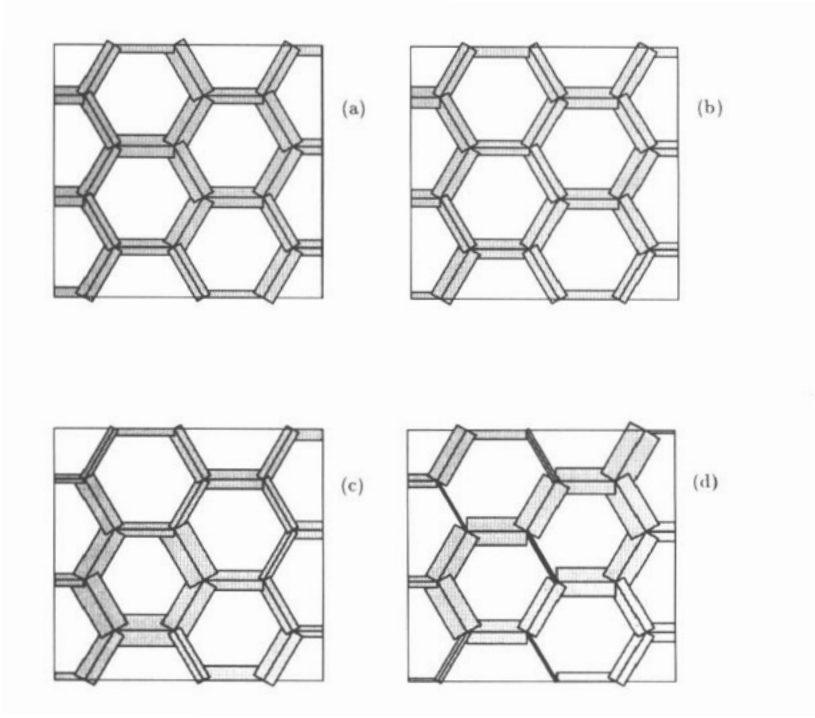


**Figure 10.** Different realizations of random variations in the nucleation activity $F_n$. The actual value of $F_n$ is plotted along, and on either side of, the grain boundary facet. (*a*), (*b*) $\Delta F_n/F_n^0 = 0.3$, (*c*) $\Delta F_n/F_n^0 = 0.6$, (*d*) $\Delta F_n/F_n^0 = 0.9$.

value within the interval $[F_n^0 - \Delta F_n, F_n^0 + \Delta F_n]$, where $F_n^0$ is chosen as the reference value $100N_I$. Four realizations have been considered, with values of $\Delta F_n$ in the range of $0.3F_n^0$ to $0.9F_n^0$. The resulting distributions of $F_n$ are visualized in figure 10 by plotting the values along and normal to the facet, similar to the $a/b$ plots in figures 5 and 8. For each of the

four realizations we computed the actual mean value $\overline{F}_n$ and the variance var $F_n$. The mean values remained within 10% of the reference value $F_n^0$; in the following, we shall use the variance to represent the randomness in the variation of nucleation activity. All results to be presented are for applied uniaxial tension $\Sigma_1 = 0$.

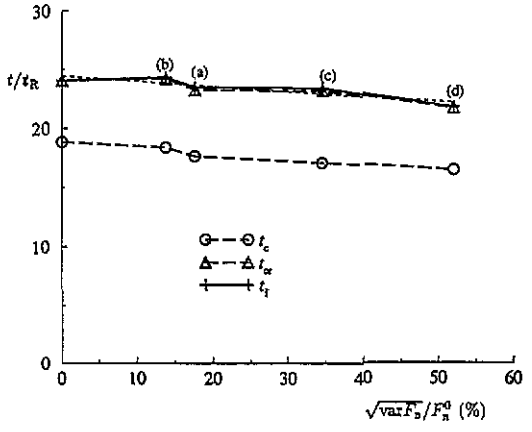


**Figure 11.** Times to first coalescence, $t_c/t_R$, times to first facet microcrack, $t_{cr}/t_R$, and times to failure, $t_f/t_R$, for (6, 5) unit cells with free grain boundary sliding and with a random variation of $F_n$. The different distributions shown in figure 10 are identified by markers (a)–(d). Results are plotted against the standard deviation in the distribution of $F_n$; the thin broken line is a linear regression of the times to failure $t_f$.

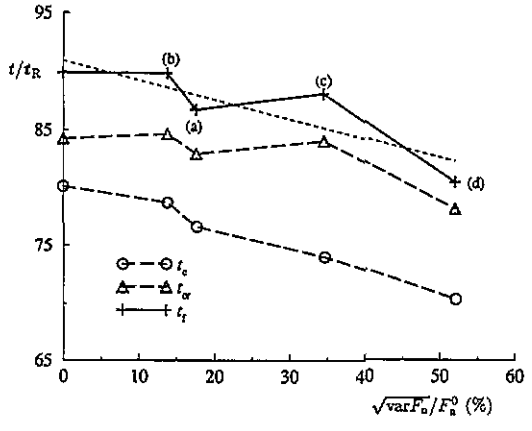


**Figure 12.** Times to first coalescence, $t_c/t_R$, times to first facet microcrack, $t_{cr}/t_R$, and times to failure, $t_f/t_R$, for (6, 5) unit cells with no grain boundary sliding and with a random variation of $F_n$. The different distributions shown in figure 10 are identified by markers (a)–(d). Results are plotted against the standard deviation in the distribution of $F_n$; the thin broken line is a linear regression of the times to failure $t_f$.

In figure 11 we again plot the three characteristic times, $t_c$, $t_{cr}$ and $t_f$, for each of the realizations shown in figure 10, along with the values for the polycrystal with

uniform nucleation activity. Completely free grain boundary sliding was assumed in the computations. We have chosen to use the standard deviation $\sqrt{\text{var } F_n}$ as the ordinate in this plot, as this turned out to give a reasonably good overall correlation. It is observed that one realization gave rise to a somewhat longer time to failure, but the general tendency is that a random variation of nucleation activity reduces the time to failure. The strongest reduction in time to failure found here is about 10%.

Again, the computations have been repeated by assuming no sliding ($\log(\dot{\epsilon}_e^C/\dot{\epsilon}_B) = 3.5$), and the results are presented in figure 12. The predicted relative reduction of the characteristic times is more or less similar to that found with completely free sliding. In this case, too, the maximum reduction in failure time is about 10%.

## 5. Discussion

The effect of random variations in the microstructure of polycrystalline aggregates has been studied here in terms of variations of the grain geometry and in terms of variations in the nucleation activity. In both cases, the mean values of either the grain geometry or the nucleation activity differed very little from those in the reference polycrystal with regular hexagonal grains and uniform properties. It has been found that any variation in microstructure leads to an enhancement of the rupture process and hence to a reduction of the lifetime; in no case did we find an increase in the lifetime.

The most interesting result of the present studies is the rather strong sensitivity of the lifetime to random variations of the grain size and shape, found in the case of freely sliding grain boundaries (figures 5 and 6). The computations show that failure occurs much earlier at grain boundary facets which are smaller than the average for the aggregate of grains considered, and that this earlier onset of failure by cavity coalescence is accompanied by a smaller total lifetime, $t_f$, for the material. This prediction of smaller times to coalescence the smaller the facet is in contrast to simple cavitation models, representing grain boundary facets as penny-shaped cracks [3, 4], since these models show increasing lifetime for decreasing facet size, as long as cavitation is creep constrained. Closer inspection of the present computational results reveals that in an array of freely sliding grains the normal force on a transverse grain boundary facet does not change much when the facet size is reduced, and therefore the normal stress and the corresponding rate of cavitation are higher on the small facet.

In an earlier study [8] for the planar multi-grain cell model with a periodic array of regular hexagonal grains, more rapid cavity nucleation has been assumed on one grain boundary facet, and the time to first coalescence on this facet has been compared with the time to final failure, where microcracks link up. In the present investigation for random grain sizes and shapes no such imperfection of the nucleation amplitude is assumed, and figure 5 illustrates that here microcracks form first at the small grain boundary facets, wherever they are located in the unit cell. Thus, in the present computations (e.g. figure 6) the limit $\Delta\rho/\rho_0 = 0$, i.e. regular hexagonal grains, represents a case where cavities nucleate and grow at the same rate on all facets normal to the maximum tensile stress. The ratio of the time to final coalescence and the final failure time, $t_c/t_f$, is determined for each of the random grain arrays (e.g. figure 6), and it is noted that this ratio varies a great deal from case to case.

In the absence of grain boundary sliding, figures 8 and 9, much less sensitivity to random variations of grain size and shape is found, and the preference for early failure at special facets is less pronounced. It is noted by comparing figures 8 and 5 that the facets subject to

first coalescence in the case of no sliding are completely different from those in the case of free sliding. In fact, figure 8 indicates that larger facets tend to fail first, which is consistent with the predictions of simple cavitation models [3, 4].

A general feature of the results shown here is that any deviation from a uniform periodic hexagonal array of grains seems to give a small increase of the facet density $\rho$ and a certain acceleration of failure. Thus, figures 6, 7 and 9 show reasonably good correlation between failure times and different measures of the average facet density, even though there is a great deal of scatter. Cavitation on facets that are close to normal to the principal tensile stress do cavitate faster than facets that are inclined, but our results do not suggest that the failure times correlate significantly better with the component of the density tensor $\alpha_{ij}$ in that direction than with the scalar density $\rho$.

The random variations of the nucleation amplitudes $F_n$ considered in figures 10–12 include rather large deviations from the average value, and it is noteworthy that the corresponding failure times differ rather little. Both for free sliding and in the absence of sliding the maximum reduction of the lifetime found here is about 10%.

Based on the present computations it can be concluded that failure times obtained by analysing a periodic array of uniform hexagonal grains give a reasonable estimate for a real material with random grain sizes and shapes if there is essentially no grain boundary sliding; but in the case of free sliding the actual failure time may be significantly overestimated. It should be emphasized that all results in the present paper are obtained for a particular, rather high, rate of grain boundary diffusion, specified by $(a/L)_I = 0.025$, which results in creep-constrained cavitation. Other values of $(a/L)_I$ may give different sensitivity to randomness of grain size and shape, but it is expected that the creep-constrained cases represent the higher sensitivity.

## References


[1] Cocks A C F and Ashby M F 1982 *Progr. Mater. Sci.* **27** 189
[2] Argon A S 1982 *Recent Advances in Creep and Fracture of Engineering Materials and Structures* ed B Wilshire and D R J Owen (Swansea: Pineridge) pp 1–52
[3] Rice J R 1981 *Acta Metall.* **29** 675
[4] Tvergaard V 1984 *J. Mech. Phys. Solids* **32** 373
[5] Tvergaard V 1985 *J. Mech. Phys. Solids* **33** 447
[6] van der Giessen E and Tvergaard V 1991 *Int. J. Frac.* **48** 153
[7] van der Giessen E and Tvergaard V 1991 *Mechanics of Creep Brittle Materials* vol 2, ed A C F Cocks and A R S Ponter (Amsterdam: Elsevier) pp 134–45
[8] van der Giessen E and Tvergaard V 1994 *Acta Metall. Mater.* 42 959
[9] van der Giessen E and Tvergaard V 1994 *Mech. Mater.* **17** 47
[10] Hsia K J, Parks D M and Argon A S 1991 *Mech. Mater.* **11** 43
[11] Ashby M F 1972 *Surf. Sci.* **31** 498
[12] Raj R and Ashby M F 1971 *Metall. Trans.* 2 1113
[13] Ghahremani F 1980 *Int. J. Solids Struct.* **16** 847
[14] Hull D and Rimmer D E 1959 *Phil. Mag.* **4** 673
[15] Chen I-W and Argon A S 1981 *Acta Metall.* **29** 1321
[16] Needleman A and Rice J R 1980 *Acta Metall.* **28** 1315
[17] Sham T-L and Needleman A 1983 *Acta Metall.* **31** 919
[18] Dyson B F 1976 *Metal Sci.* **10** 349
[19] Dyson B F 1983 *Scr. Metall.* **17** 31
[20] Sklenička V, Saxl I and Čadek J 1991 *Mechanics of Creep Brittle Materials* vol 2, ed A C F Cocks and A R S Ponter (Amsterdam: Elsevier) pp 242–53
[21] Budiansky B and O'Connell R J 1976 *Int. J. Solids Struct.* **12** 81
[22] Kachanov M 1992 *Appl. Mech. Rev.* **45** 304
[23] Anderson P M and Rice J R 1985 *Acta Metall.* **33** 409
[24] Peirce D, Shih C F and Needleman A 1984 *Comput. Struct.* **18** 875